arXiv:1605.00850v1 [cond-mat.mes-hall] 3 May 2016

Out-of-plane spin polarization of edge currents in Chern insulator with Rashba spin-orbit interaction

Tsung-Wei Chen,[1,*] Chin-Lun Hsiao,[1,2] and Chong-Der Hu[2]

[1]*Department of Physics, National Sun Yat-sen University, Kaohsiung 80424, Taiwan*
[2]*Department of Physics and Center for Theoretical Sciences, National Taiwan University, Taipei 106, Taiwan*

(Dated: May 4, 2016)

We investigate the change in the non-zero Chern number and out-of-plane spin polarization of the edge currents in a honeycomb lattice with the Haldane-Rashba interaction. This interaction breaks the time-reversal symmetry due to the Haldane phase caused by a current loop at site-I and -II atoms and also accounts for the Rashba-type spin-orbit interaction. The Rashba spin-orbit interaction increases the number of Dirac points and the band-touching phenomenon can be generated by tuning the on-site potential in the non-zero Haldane phase. By using the Pontryagin winding number and numerical Berry curvature methods, we find that the Chern number pattern is $\{+2,-1,0\}$ and $\{-2,+1,0\}$ for the positive and negative Haldane phase, respectively. A non-zero Chern number is called a Chern-insulating phase. We discovered that changes in both the Haldane phase and on-site potential leads to a change in the orientation of the bulk spin polarization of site-I and site-II atoms. Interestingly, in a ribbon with a zigzag edge, which naturally has site-I atoms at one outer edge and site-II atoms at the opposite outer edge, the spin polarization of the edge states approximately obeys the properties of bulk spin polarization regardless of the change in the Chern number. In addition, even when the Chern number changes from $+2$ to -1 (or -2 to $+1$), by tuning the strength of the on-site potential, the sign of the spin polarization of the edge states persists. This approximate bulk-edge correspondence of the spin polarization in the Haldane-Rashba system would play an important role in spintronics, because it enables us to control the orientation of the spin polarization in a single Chern-insulating phase.

PACS numbers: 71.70.Ej, 72.25.Dc, 73.43.Cd, 85.75.-d

I. INTRODUCTION

The classification of matter by using various topological properties of the band structure has become a central subject in condensed matter physics. The Berry curvature[1] embedded within the band structure plays an important role in constructing various topological indices.

Thus, it was found that the quantized Hall conductance in the integer quantum Hall regime can be determined by the topological index Chern number (Ch) or TKNN integer [2], which was shown to be the integral of the Berry curvature over the Brillouin zone of the bulk system. A change in the Chern number corresponds to a change in the number of edge currents, which is the bulk-edge correspondence [3]. Importantly, in Ref. [4], Haldane proposed a time-reversal-symmetry-broken two-band model that exhibits an energy gap without Landau levels in the bulk and gapless excitation at the edge of a honeycomb lattice, the so-called Chern insulator. The variation in the Chern number is due to a band-touching phenomenon, in which the energy gap of the bulk system closes and opens at some Dirac points in the Brillouin zone. In this sense, the band-touching phenomenon, generated by different mechanisms, would lead to different topological phases. Accounting for the spin-orbit interaction, the combination of a Chern insulator and its time-reversal pair results in the quantum-spin Hall phase in graphene (Kane-Mele model) [5] and HgTe quantum wells (BHZ model) [6] in a two-dimensional system. This time-reversal-invariant quantum spin Hall insulator composed of two time-reversal-breaking Chern insulators has been generalized to three-dimensional systems, where it is called a topological insulator [7]. This was later confirmed experimentally [8]. The topological phases of the time-reversal invariant system can be determined by calculating the Z_2 topological index of the bulk system [9] or the spin Chern number [10–13]. On the other hand, a quantum anomalous Hall phase can be exhibited in graphene with a Rashba spin-orbit interaction in the presence of an exchange field [14].

It was theoretically proposed that in a honeycomb lattice with a Kane-Mele Hamiltonian including the Rashba spin-orbit interaction, the quantum spin Hall phase persists in the presence of an exchange field, i.e., the time-reversal symmetry is broken [15, 16]. In Ref. [17], it was demonstrated that the edge state in the quantum spin Hall phase can persist even for a strong magnetic field.

Moreover, because the spin-orbit interaction relates to the orbital motion of the electron, a change in the Chern number from positive to negative integer leads to a change in the direction of the edge current, and the out-of-plane spin polarization (hereafter called spin polarization for convenience) may change due to the spin-orbit

*Electronic address: twchen@mail.nsysu.edu.tw

coupling. However, this is not always true because the spin polarization of the edge states would also be affected by the on-site potential, as in the honeycomb lattice. The edge current is exhibited by the Haldane current loops at site-I or site-II atoms. The zigzag ribbon naturally has site-I atoms at one outer edge and site-II at the opposite outer edge. This implies that the two Haldane current loops must contribute unequally to the edge currents [see Fig. 1(a)], and that one of the two Haldane current loops would dominate at one edge. At right (left) side of the ribbon, the site-I (site-II) atoms has more nearest neighbor atoms than site-II (site-I) atoms. Because the Rashba spin-orbit interaction governs the nearest neighbor hopping of different sites, this implies that the two different sites must contribute unequally to the spin polarization of edge currents. Furthermore, different spin states at the edges of a honeycomb lattice with a zigzag edge would occupy different sites under broken time reversal symmetry. Thus, the on-site potential would behave like an effective magnetic field for the edge states. As a result, the bulk spin polarization for site-I and site-II atoms would have the same behavior as the spin polarization of edge currents. In a manner similar to the bulk-edge correspondence in the Chern number, there would be an approximate bulk-edge correspondence for spin polarization. Therefore, if the band-touching phenomenon is caused by the on-site potential, a question arises naturally: Can the spin polarization of the edge currents also be protected in the time-reversal-symmetry-broken system with a spin-orbit interaction under a change in the Chern number?

Furthermore, in Ref. [18], the authors proposed a scheme to realize the Haldane model by using ultracold atoms trapped in an optical lattice. Later, the detection of the topological phase of a Chern insulator was proposed in Ref. [19]. Recently, it was shown experimentally that the Haldane model can be exhibited with ultracold fermions [20].

Motivated by these issues, in this paper, we study a Haldane system with Rashba spin-orbit interaction [21] in a honeycomb lattice, from now on called a Haldane-Rashba system. The change in the Chern number in the Haldane system generated by the on-site potential is known to be $\{-1, 0\}$ and $\{+1, 0\}$ for a negative and positive Haldane phase, respectively. A non-zero Chern number is called a Chern-insulating phase. The number of Dirac points of the Haldane system is 2 in the Brillouin zone (see Fig. 2). On the other hand, the number of Dirac points in the pure Rashba system is 6 in the honeycomb lattice [21] [see Fig. 1(b)]. We will show that in the Haldane-Rashba system the resulting Chern number patterns are $\{-2, +1, 0\}$ and $\{+2, -1, 0\}$ for a negative and positive Haldane phase, respectively. Therefore, the Haldane-Rashba system would be a candidate for the investigation of the persistence of spin polarization of the edge states under a change in the Chern number. We will show that the spin-polarization of the edge currents persists under the change in Chern number and furthermore that the magnitude of the spin polarization can be tuned by the on-site potential. This implies that we could control the orientation of the spin polarization of the edge currents in a single Chern-insulating phase.

This paper is organized as follows. In section II, we introduce the Haldane-Rashba system. We map the honeycomb lattice to a square lattice and find the Dirac points. In section III, we obtain the Chern number pattern of the Haldane-Rashba system by using the Pontryagin winding number method and numerically calculating the Berry curvature. In section IV, we study the spin polarization of the bulk and edge states. The conclusion is given in section V.

II. DIRAC POINTS IN THE HALDANE-RASHBA SYSTEM

In this section, we study the number of Dirac points in the Haldane-Rashba system in the square Brillouin zone transformed from the honeycomb lattice. The Haldane-Rashba Hamiltonian is given by

$$\begin{aligned} H =& t \sum_{<i,j>} c^{\dagger}_{i\sigma} c_{j\sigma} + t_2 \sum_{\ll i,j \gg, \sigma} e^{-i\nu_{ij}\phi} c^{\dagger}_{i\sigma} c_{j\sigma} \\ &+ i\alpha \sum_{<i,j>} \sum_{\sigma\sigma'} (\mathbf{s} \times \mathbf{d}_{ij})^{\sigma\sigma'}_{z} c^{\dagger}_{i\sigma} c_{j\sigma'} + G \sum_{i\sigma} \xi_i c^{\dagger}_{i\sigma} c_{i\sigma}, \end{aligned} \tag{1}$$

where $< i, j >$ represents the nearest-neighbor hopping, $\sigma = \uparrow, \downarrow$ the up and down spin states, and $\ll i, j \gg$ the next nearest-neighbor hopping. The vector $\mathbf{s}$ are the Pauli matrices. The indices i, j corresponds to site-I or site-II atoms. The first term of Eq. 1) is the tight-binding Hamiltonian of the honeycomb lattice. The second and third terms of Eq. (1) are the Haldane and Rashba Hamiltonians, respectively. The factor ν_{ij} is the sign of the current loop $\mathbf{d}_{I,II} \times \mathbf{d}_{II,I}$ or $\mathbf{d}_{II,I} \times \mathbf{d}_{I,II}$ as shown in the dashed lines of Fig. 1(a). The fourth term of Eq. (1) is the on-site potential, which can be experimentally realized [20]. $\xi_I = +1$ and $\xi_{II} = -1$ are for site-I and site-II atoms, respectively. The on-site potential term $G \sum_{i\sigma} \xi_i c^{\dagger}_{i\sigma} c_{i\sigma}$ generates the band-touching phenomenon and plays the key role for the physics discussed in this paper [see IV].

Using $q_1 = \mathbf{k} \cdot \mathbf{a}_1$ and $q_2 = \mathbf{k} \cdot \mathbf{a}_2$, Eq. (1) can be written as

$$H = \begin{pmatrix} G + Z_+ & X + iY & 0 & iR_- \\ X - iY & -G + Z_- & -iR^*_+ & 0 \\ 0 & iR_+ & G + Z_+ & X + iY \\ -iR^*_- & 0 & X - iY & -G + Z_- \end{pmatrix}, \tag{2}$$

where the wave vector is $(c^{\dagger}_{\mathbf{k}I\uparrow}, c^{\dagger}_{\mathbf{k}II\uparrow}, c^{\dagger}_{\mathbf{k}I\downarrow}, c^{\dagger}_{\mathbf{k}II\downarrow})^T$ and $Z_+ = 2t_2 [\cos(q_1 - \phi) + \cos(q_2 + \phi) + \cos(q_2 - q_1 - \phi)]$, $Z_- = 2t_2 [\cos(q_1 + \phi) + \cos(q_2 - \phi) + \cos(q_2 - q_1 + \phi)]$, $X = t[1 + \cos(q_1) + \cos(q_2)], Y = t[\sin(q_1) + \sin(q_2)]$, $R_- = \alpha(-1 + \exp[i(q_1 - \frac{\pi}{3})] + \exp[i(q_2 + \frac{\pi}{3})])$, $R_+ =$

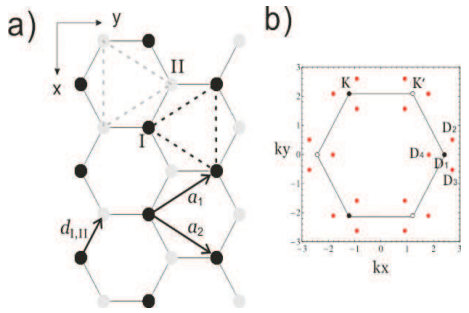

FIG. 1: (a) Honeycomb lattice and current loop (dashed lines) in the Haldane model. (b) Brillouin zone and the distribution of the Dirac points for $\alpha = 0.7t$.

TABLE I: Reciprocal lattice in **k** and **q** space

k-space	**q**-space
$\mathcal{G}_1 = (4\pi/3a)(-\sqrt{3}/2, 1/2)$	$\mathcal{G}_1 = (2\pi/a)(1, 0)$
$\mathcal{G}_2 = (4\pi/3a)(\sqrt{3}/2, 1/2)$	$\mathcal{G}_2 = (2\pi/a)(0, 1)$

$\alpha(-1 + \exp[i(q_1 + \frac{\pi}{3})] + \exp[i(q_2 - \frac{\pi}{3})])$. Using the basis vectors $\mathbf{a}_1$ and $\mathbf{a}_2$ shown in Fig. 1(a), we arrive at the transformation between the $\mathbf{q} = (q_1, q_2)$ and $\mathbf{k} = (k_x, k_y)$ spaces,

$$\begin{aligned} q_1 &= -(\sqrt{3}/2)k_x + (3/2)k_y, \\ q_2 &= (\sqrt{3}/2)k_x + (3/2)k_y. \end{aligned} \tag{3}$$

The reciprocal lattice vector $(\mathcal{G}_1, \mathcal{G}_2)$ in **q**-space transformed from **k**-space is given in Table I. Therefore, we map the honeycomb reciprocal lattice to a square lattice with the Brillouin zone boundary $q_1 \in (-\pi, \pi)$ and $q_2 \in (-\pi, \pi)$.

The eigenvalue of Eq. (2) is given by

$$E_{n\sigma} = \frac{1}{2}(Z_- + Z_+) + n\sqrt{\left(G - \frac{Z_- - Z_+}{2}\right)^2 + \frac{\mathcal{D}_\sigma}{2}}, \tag{4}$$

where $n = \pm$, $\sigma = \pm$, and

$$\begin{aligned} \mathcal{D}_\pm =& |R_-|^2 + |R_+|^2 + 2|X_0|^2 \\ & \pm \sqrt{(|R_-|^2 - |R_+|^2)^2 + 4|R_- X_0^* - R_+^* X_0|^2}, \end{aligned} \tag{5}$$

with $X_0 = X + iY$. We note that $\mathcal{D}_\pm$ is independent of the Haldane hopping interaction t_2 and the Haldane phase ϕ. The lower of the two conduction bands is E_{+-}, and the upper of the two valence bands is E_{--}. The band gap of the Haldane-Rashba system is thus given by

$$E_g = 2\sqrt{\left(G - \frac{Z_- - Z_+}{2}\right)^2 + \frac{\mathcal{D}_-}{2}}. \tag{6}$$

The Chern number changes when the band-touching phenomenon occurs. In this case, we tune the on-site potential to change the band gap. It can be shown that $\mathcal{D}_-$ is always positive in the Brillouin zone and hence, $E_g = 0$ leads to the result,

$$G = \frac{Z_- - Z_+}{2}, \quad \mathcal{D}_- = 0. \tag{7}$$

The condition $\mathcal{D}_- = 0$ can be simplified to the result

$$|R_- R_+ + X_0^2|^2 = 0. \tag{8}$$

The dashed lines shown in Fig. 2(a) are obtained from Eq. (8), which provides the possible locations of the Dirac points. In this paper, we consider only small positive values of α ($0 < \alpha < t$)[14, 21]. In the absence of a Rashba spin-orbit interaction, $\mathcal{D}_\pm = 2|X_0|^2$. The energy gap is then given by $E_g = \sqrt{(G - (Z_- - Z_+)/2)^2 + |X_0|^2}$. If we would like to tune the on-site potential G to construct the band-touching phenomenon, then $E_g = 0$ leads to the solution $G = (Z_- - Z_+)/2 + \sqrt{-|X_0|^2}$. Thus, the Dirac points are determined by $|X_0|^2 = 0$, which can also be obtained from Eq. (8). The Dirac points for the Haldane system are the set of K points $(2\pi/3, -2\pi/3)$, $(4\pi/3, 2\pi/3)$, and $(-2\pi/3, -4\pi/3)$ and the set of K' points $(-2\pi/3, 2\pi/3)$, $(2\pi/3, 4\pi/3)$, and $(-4\pi/3, -2\pi/3)$. In the Brillouin zone, the Dirac points in the Haldane system are $(\pm 2\pi/3, \mp 2\pi/3)$, as shown in Fig. 2(b). One Dirac point is located at **q** and the other at $-\mathbf{q}$. The two Dirac points form a Dirac pair. In the presence of the Rashba spin-orbit interaction, besides the Dirac pair

$$D_1 : (-2\pi/3, 2\pi/3), D_1' : (2\pi/3, -2\pi/3) \tag{9}$$

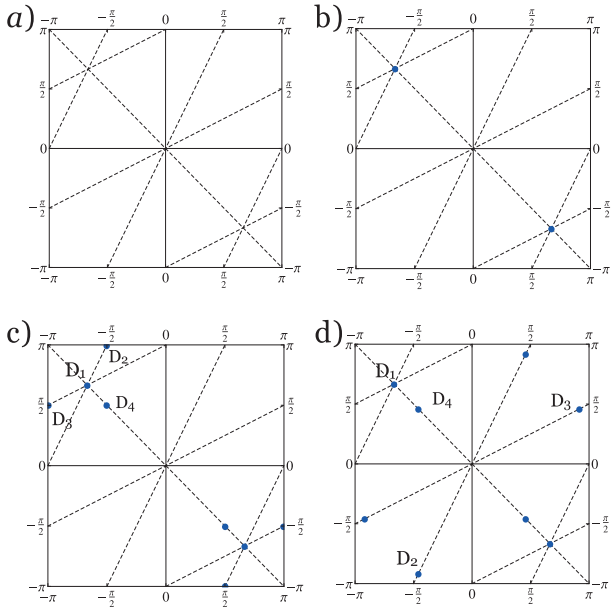

FIG. 2: The Dirac points (filled circles) in the Brillouin zone. (a) the Brillouin zone and the dashed line determined by Eq. (8), (b) the two Dirac points in the Haldane system, (c) the eight Dirac points in the Haldane-Rashba system with $0 < \alpha < 1/\sqrt{2}$, and (d) the eight Dirac points in the Haldane-Rashba system with $\alpha > 1/\sqrt{2}$.

there are six other Dirac points, shown in Fig. 2(c) and (d)[see Fig. 1(b) in k space]. Furthermore, we note that when the Rashba interaction is increased, the Dirac points D_2 and D_3 (and their Dirac pair partners) approach the Brillouin zone boundary and appear in the Brillouin zone as shown in Fig. 2(c) and (d). The strength of the Rashba interaction is $\alpha_c = 1/\sqrt{2}$. For $\alpha < \alpha_c$, three of the six Dirac points satisfying Eq. (8) are given by $D_i : (q_1^0, q_2^0)$,

$$D_2 : (-\theta_0, 2(\pi-\theta_0)),\ D_3 : (2(\theta_0-\pi), \theta_0),\ D_4 : (-\theta_0, \theta_0), \tag{10}$$

where

$$\theta_0 = \cos^{-1}\left(\frac{2(\alpha/t)^2 - 1}{2(\alpha/t)^2 + 2}\right), \tag{11}$$

and the other three Dirac points are given by D_i' : $(-q_1^0, -q_2^0)$. Based on the dashed line satisfying Eq. (8) and shown in Fig. 2, the eight Dirac points in the Haldane-Rashba system are shown in Fig. 2(c). For $\alpha > \alpha_c$, we have

$$D_2 : (-\theta_0, -2\theta_0),\ D_3 : (2\theta_0, \theta_0),\ D_4 : (-\theta_0, \theta_0). \tag{12}$$

In the next section, we will obtain the Chern number pattern of the Haldane-Rashba system by investigating the band-touching phenomenon of these eight Dirac points. For convenience, we scale the energy by the hopping energy t, i.e., we set $t = 1$ in the following calculations.

III. CHERN NUMBER PATTERN AND EDGE STATES

In this section, we will obtain the Chern number pattern of the Haldane-Rashba system. First, we construct an effective two-band model from the Hamiltonian Eq. (2) to map the $\mathbf{q}$ space to the $\mathbf{d}(\mathbf{q})$ space and calculate the Pontryagin winding number wrapped by the $\mathbf{d}$ vector. We also use the Berry curvature method to present the numerical result of the Chern number pattern. The resulting edge states are also discussed in this section.

Equation (8) determines the locations of the Dirac points. This implies that the four-band Haldane-Rashba Hamiltonian can be cast as an effective two-band model for determining the Chern number pattern

$$H_{\rm eff} = \begin{pmatrix} d_z & d_x - id_y \\ d_x + id_y & -d_z \end{pmatrix}. \tag{13}$$

The Chern number for the two-band model can be determined by the Pontryagin winding number method [22, 23]

$$\mathrm{Ch} = \frac{1}{2}\sum_{\mathbf{q}\in D_i, D_i'} \mathrm{sgn}\Big(\frac{\partial \mathbf{d}}{\partial q_1}\times\frac{\partial \mathbf{d}}{\partial q_2}\Big)_z \mathrm{sgn}(d_z), \tag{14}$$

where $\mathrm{sgn}(\cdots)$ indicates the sign of $(\cdots)$, z an arbitrary axis selected in this pseudo-spin space, and D_i a set of Dirac points in the Brillouin zone [1]. The two terms d_x and d_y determine the positions of the Dirac points by the requirements $d_x = 0$ and $d_y = 0$. Equation (8) is equivalent to the vanishing real as well as imaginary part of $R_-R_+ + X_0^2$. Because Eq. (14) requires only the sign of each term in the bracket, the terms d_x, d_y, and d_z accounting for Eq. (8) can be chosen as

$$\begin{aligned} d_x &= \sqrt{\tilde{d}_x},\ \tilde{d}_x = \mathrm{Re}[R_-R_+ + X_0^2], \\ d_y &= \sqrt{\tilde{d}_y},\ \tilde{d}_y = \mathrm{Im}[R_-R_+ + X_0^2], \\ d_z &= G - (Z_- - Z_+)/2. \end{aligned} \tag{15}$$

Substituting Eqs. (9) and (10) [or Eqs. (9) and (12)] in d_z, we derive

$$\begin{aligned} d_z(D_1) &= G - G_e\sin\phi,\ d_z(D_{2,3,4}) = G - M_\alpha\sin\phi \\ d_z(D_1') &= G + G_e\sin\phi,\ d_z(D_{2,3,4}') = G + M_\alpha\sin\phi, \end{aligned} \tag{16}$$

where $M_\alpha = G_eG_\alpha$ and (note that $t = 1$ was used)

$$G_e = 3\sqrt{3}t_2,\ G_\alpha = \frac{\sqrt{1+4\alpha^2}}{(1+\alpha^2)^2}. \tag{17}$$

On the other hand, we note that $R_-R_+ + X_0^2$ vanishes at the Dirac points. The ambiguity appearing in the denominator after a partial derivative with respect to $\mathbf{q}$ should be neglected in the sign function. The sign of the term $(\partial_{q_1}\mathbf{d}\times\partial_{q_2}\mathbf{d})_z$ can be determined by $(\partial_{q_1}\tilde{\mathbf{d}}\times\partial_{q_2}\tilde{\mathbf{d}})_z$, where $\tilde{\mathbf{d}} = (\tilde{d}_x, \tilde{d}_y)$ [see Eq. (15)]. Substituting Eqs. (9) and (10) [or Eqs. (9) and (12)] in $J_z \equiv (\partial_{q_1}\tilde{\mathbf{d}}\times\partial_{q_2}\tilde{\mathbf{d}})_z$, we have

$$\begin{aligned} J_z(D_1) &= (9\sqrt{3}/2)\alpha^4,\ J_z(D_{2,3,4}) = -(27\sqrt{3}/2)\alpha^4G_\alpha \\ J_z(D_1') &= -(9\sqrt{3}/2)\alpha^4,\ J_z(D_{2,3,4}') = (27\sqrt{3}/2)\alpha^4G_\alpha. \end{aligned} \tag{18}$$

Using Eqs. (16) and (18), we can calculate the Chern number in each zone enclosed by the phase boundary. For example, considering $0 < \phi < \pi$, the result is given in Table II.

Note that α^4 and G_α are always positive, and the sign of J_z can easily be obtained from Eq. (18) at each Dirac point. Substituting Eqs. (16) and (18) into Eq. (14) and

[1] The overall sign of the Chern number in Eq. (14) depends on the Jacobian transformation and the overall sign chosen in d_y and d_x. However, the overall sign choice does not alter the conclusion of this paper. The Jacobian transformation from (k_x, k_y) to (q_1, q_2) is $+1$, and thus, in this paper, we choose the same sign convention for d_x and d_y as in Ref. [4]

TABLE II: Values of the Chern number Ch in a Haldane-Rashba system with $0 < \phi < \pi$.

Dirac points	D_1	$D_{2,3,4}$	D_1'	$D_{2,3,4}'$	Ch
Mass	$G-G_e$	$G-M_\alpha$	$G+G_e$	$G+M_\alpha$	
$\mathrm{sgn}(J_z)$	+	−	−	+	
$\mathrm{sgn}(J_z)\mathrm{sgn}(d_z)$					
$G<-G_e$	−	+	+	−	0
$-G_e<G<-M_\alpha$	−	+	−	−	−1
$-M_\alpha<G<M_\alpha$	−	+	−	+	+2
$M_\alpha<G<G_e$	−	−	−	+	−1
$G_e<G$	+	−	−	+	0

summing over these eight Dirac points, we obtain

$$\mathrm{Ch} = \frac{1}{2}\left[\mathrm{sgn}\left(G-G_e\sin\phi\right)-\mathrm{sgn}\left(G+G_e\sin\phi\right)\right] + \frac{3}{2}\left[\mathrm{sgn}\left(G+M_\alpha\sin\phi\right)-\mathrm{sgn}\left(G-M_\alpha\sin\phi\right)\right]. \quad (19)$$

Therefore, the phase diagram of the Haldane-Rashba system can be determined by Eqs. (19) and (17). The result is shown in Fig. 3(a). The Haldane-Rashba system exhibits the Chern number pattern $\{+2,-1,0\}$ and $\{-2,+1,0\}$ for a positive and negative Haldane phase, respectively. A system state with a non-zero Chern number is called a Chern-insulating state. There are two boundaries exhibited by the two parameters M_α and G_e. Furthermore, the change in Chern number is $\Delta\mathrm{Ch} = \pm N$, where N is the number of Dirac points occurring simultaneously in a band-touching phenomenon [4, 24]. It is interesting to note that when the Chern number changes from $+2$ to -1 (or -2 to $+1$), the band-touching phenomenon occurs at the three Dirac points D_2, D_3, and D_4 simultaneously, as shown in Fig. 3(c) and (d) and theoretically confirmed in Table II. The simultaneous band touching leads to the resulting coefficient 3/2 in the second square bracket of Eq. (19), which is three times larger than the band touching caused by G_e. Interestingly, it was recently found that the shape of the Dirac cone is related to the spin connection that couples to the sublattice pseudospin [25]. On the other hand, when $\alpha = 0$, the Chern number becomes $\mathrm{Ch} = \mathrm{sgn}(G+G_e\sin\phi) - \mathrm{sgn}(G-G_e\sin\phi)$, which is doubled because the electron spin is considered. When $t_2 = 0$, Eq. (19) gives $G_e = 0$ and $M_\alpha = 0$, and thus, $\mathrm{Ch} = 0$, which is in agreement with the fact that the Chern number vanishes in the time-reversal symmetric system.

In order to compare the present result obtained in $\mathbf{q}$ space, we also calculate the Chern number numerically by using the Berry curvature method in $\mathbf{k}$ space,

$$\mathrm{Ch} = -\frac{1}{2\pi}\sum_n \int_{BZ} \Omega_{xy}^{(n)}(\mathbf{k})dk_x dk_y, \quad (20)$$

where

$$\Omega_{xy}^{(n)} = \sum_{n'(\neq n)} \frac{2\mathrm{Im}\langle\psi_{nk}|\frac{\partial H}{\partial k_x}|\psi_{n'k}\rangle\langle\psi_{n'k}|\frac{\partial H}{\partial k_y}|\psi_{nk}\rangle}{(E_{n'}(\mathbf{k})-E_n(\mathbf{k}))^2}. \quad (21)$$

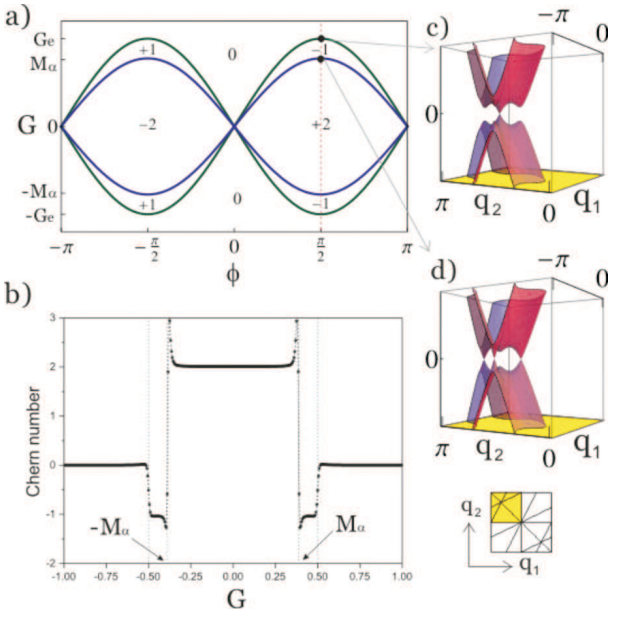

FIG. 3: (Color online) (a) The phase diagram and (b) the numerical result of the Chern number pattern of the Haldane-Rashba system. The band structures at the phase boundary is shown in (c) and (d). We have drawn the band structure at only one quadrant of the Brillouin zone to show the occurrence of the band-touching phenomenon. The band structure at the opposite quadrant is fully gapped.

We consider the Haldane-Rashba system with $\phi = \pi/2$, $\alpha = 0.7$, and $t_2 = 1/(6\sqrt{3})$. We have $G_e = 0.5$ and $M_\alpha \simeq 0.38$. The result is shown in Fig. 3 (b), which is in agreement with our Pontryagin winding number method.

We also numerically calculate the upper one of two valence bands and the lower one of the two conduction bands in order to check the band-touching phenomenon. In the change of total Chern number from -1 to $+2$, we find that the upper one of two valence bands ($\mathrm{Ch} = -1$) increases by 3 and becomes $+2$, and the lower one of two conduction bands ($\mathrm{Ch} = +1$) decreases by 3 and becomes -2. The Chern number of the lower one of two valence bands is numerically found to be always zero, and the total Chern number of the two valence bands indeed changes from -1 to $+2$.

Next, we turn to the discussion of the resulting edge states in the Haldane-Rashba system. We consider the strength of the Rashba spin-orbit interaction $\alpha = 0.7$ ($M_\alpha = 0.38$), $t_2 = 1/(6\sqrt{3})$ ($G_e = 0.5$), and fix the two Haldane phases at $\phi = \pi/2$ and $\phi = -\pi/2$. Tuning the on-site potential G, we get the Chern number pattern $\{+2,-1,0\}$ for the positive Haldane phase $\phi = +\pi/2$ for which the phase transition occurs at $G = \pm M_\alpha$ [obtained from Eq. (17)] for $\{+2,-1\}$ and $G = \pm G_e$ for $\{-1,0\}$. The edge states and the corresponding wave function distribution $|\psi|^2$ for the Chern numbers $+2$ and -1 are shown in Fig. 4(a) and (b).

Figure 4(a) and (b) show the edge states and their

wave function distributions at the positive Haldane phase $\phi = \pi/2$, which is located explicitly at the edge of the honeycomb ribbon. Based on the slope of each edge state in the band structure, the current flow could be obtained. The edge states D, B are located at the right hand side of the ribbon and A, C at the left hand side. The Chern number of Fig. 4(a) is thus identified as $+2$. When the on-site potential changes from $G = 0.1$ to $G = 0.45$ passing through $G = 0.38$, a phase transition occurs and the edge state BD (AC) reduces to the edge state A' (B') as shown in Fig. 4(b). There the Chern number now becomes -1. For the negative Haldane phase $\phi = -\pi/2$ [see Fig. 4(c) and (d)], the edge states AC and B' are located at the right hand side and BD and A' at the left hand side of the ribbon, respectively.

Thus, we have obtained the Chern number pattern and determined the regime of each Chern-insulating phase of the Haldane-Rashba system. We used the Pontryagin winding number method in $\mathbf{q}$ space to determine the Chern number and the phase boundary, and the result is in agreement with the numerical method calculated in $\mathbf{k}$ space. In the next section, we study the variation of the spin-polarization of the edge states across the phase boundary.

IV. SPIN POLARIZATION OF EDGE STATES

Because the edge current is non-zero in the Chern insulating states, the interplay of orbital motion (current loop formed by the edge currents) and the Rashba spin-orbit interaction may cause a non-zero out-of-plane spin polarization. We note that the zigzag graphene ribbon naturally form site-I atoms (more neighbors of site-II atoms) at the right hand and site-II atoms (more neighbors of site-I atoms) at the left hand side of the ribbon, respectively [see Fig. 1]. In this sense, the two edges of the ribbon must have different Haldane current loops to exhibit an edge current, as shown in Fig. 1(a). On the other hand, the Rashba spin-orbit interaction indicates that the in-plane spin $\mathbf{s}$ interacts with the nearest-neighbor hopping vector $\mathbf{d}_{ij}$. Because the two edges of the ribbon have opposite hopping directions between site-I and site-II atoms, the cross product of the in-plane spin and nearest-neighbor hopping vectors implies that the sign of spin polarization on one side is opposite to that on the other side.

The Rashba spin-orbit coupling governs the nearest neighbor hopping of different site atoms. At right (left) side of the ribbon, the site-I (site-II) atom has more nearest neighbors than site-II (site-I) atoms. Therefore, site-I (site-II) atoms contributes more Rashba spin-orbit hopping to the site-II atoms at right (left) hand side of ribbon. Therefore, the spin polarization of the edge states at the right (left) hand side of the ribbon would be dominated by site-II (site-I) atoms.

Furthermore, we note that the on-site potential at site-II is negative compare to that at site-I. The effective Hamiltonian for the edge states would be $Gc^{\dagger}_{I,\sigma}c_{I,\sigma}$ for the left hand side and $-Gc^{\dagger}_{II,-\sigma}c_{II,-\sigma}$ for the right hand side of the ribbon, where $-\sigma$ means the opposite spin states with respect to σ. When the on-site potential is turned on, the interplay of the Haldane phase and the on-site potential would cause the site-I and site-II atoms to contribute unequally to the out-of-plane spin polarization of the edge currents.

Interestingly, this also indicates that the on-site potential behaves like an effective magnetic field for the edge currents. In this sense, when the sign of the on-site potential is changed, the spin polarization also changes its sign regardless of the change in the Chern number. Furthermore, this also implies that the magnitude of the spin polarization at both edges should also grow with the on-site potential. Consequently, the spin-polarization would persist under a change in the Chern number. In order to show these bulk and edge effects, we first study the bulk spin polarization and then compare the result to that of the edge currents. The spin matrices for site-I and site-II are given by S^I_z and S^{II}_z, respectively,

$$S^I_z = \begin{pmatrix} 1 & 0 & 0 & 0 \\ 0 & 0 & 0 & 0 \\ 0 & 0 & -1 & 0 \\ 0 & 0 & 0 & 0 \end{pmatrix}, \; S^{II}_z = \begin{pmatrix} 0 & 0 & 0 & 0 \\ 0 & 1 & 0 & 0 \\ 0 & 0 & 0 & 0 \\ 0 & 0 & 0 & -1 \end{pmatrix}. \quad (22)$$

The on-site potential would effectively couple to the spins of the edge states at site-I and -II with $-S^I_z$ and S^{II}_z, respectively. The linear responses of spin $\Sigma^{I,II}_z = (\hbar/2)S^{I,II}_z$ to an applied electric field in the y direction E_y is denoted as $\langle\Sigma^{I,II}_z\rangle = (e\hbar/8\pi)\langle S^{I,II}_z\rangle E_y$, where

$$\langle S^{I,II}_z\rangle = \frac{1}{\pi}\int_{BZ} dk_x dk_y \times \sum_{n\neq n'} \frac{\mathrm{Im}\langle\psi_{nk}|S^{I,II}_z|\psi_{n'k}\rangle\langle\psi_{n'k}|\frac{\partial H}{\partial k_y}|\psi_{nk}\rangle}{(E_{n'}(\mathbf{k}) - E_n(\mathbf{k}))^2}. \quad (23)$$

$\langle S^I_z\rangle$ and $\langle S^{II}_z\rangle$ in Eq. (23) are calculated numerically and shown in Fig. 5 where the Rashba spin-orbit interaction $\alpha = 0.7$. When the on-site potential is fixed and non-zero, the change in the Haldane phase changes the magnitude of the bulk spin polarization. When the sign of the Haldane phase is changed, the sign of the spin polarization also changes because of the Rashba spin-orbit interaction, as shown in Fig. 5(a). The inset in Fig. 5(a) indicates the outer boundary points for the change in Chern number. In Fig. 5(a), we only show the effect of on-site potential for $-\langle S^I_z\rangle$. The result for $\langle S^{II}_z\rangle$ can be obtained by replacing $\phi \to -\phi$ and $G \to -G$ as can be seen in Eq. (2). When varying the on-site potential, the number of edge states and the current direction would change.

The sign of the bulk spin polarization is approximately determined by the sign of the Haldane phase in the regimes of non-zero Chern number. For instance, when $\phi > 0$ ($\phi < 0$), $-\langle S^I_z\rangle$ is negative (positive) and, as shown

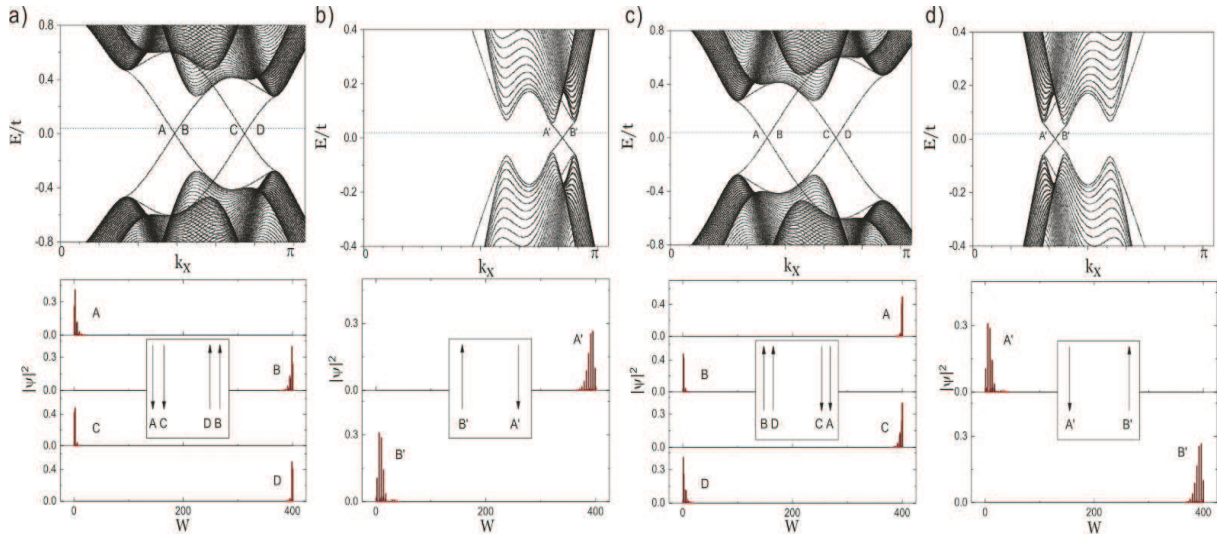

FIG. 4: Edge state and the corresponding wave function distribution and the current direction of the Haldane-Rashba system with $\alpha = 0.7$, $t_2 = 1/(6\sqrt{3})$, and $E_F = 0.01$ for (a) $G = 0.1t$, (b) $G = 0.45t$ at $\phi = +\pi/2$, (c) $G = 0.1t$, and (d) $G = 0.45t$ at $\phi = -\pi/2$. The ribbon denoted W is 400 atoms wide.

in the intervals ab ($\phi > 0$) and $a'b'$ ($\phi < 0$) and the intervals cd ($\phi > 0$) and $c'd'$ ($\phi < 0$). However, when G is small and ϕ is close to 0 and π, the sign of the bulk spin polarization can not be determined only by the Haldane phase. For the interval ef, the sign of the bulk spin polarization is altered by the on-site potential, as shown in the interval ec and df for $G = 0.1$, where ϕ is close to 0 and π. This is because the Haldane hopping term $t_2 e^{i\nu_{ij}\phi} c^\dagger_{i\sigma} c_{i\sigma}$ has the same behavior (effective magnetic field) as the on-site term $G\xi_i c^\dagger_{i\sigma} c_{i\sigma}$[2]. For small G, the competition of the Haldane hopping term and the on-site term becomes explicit when ϕ is close to 0 and π.

In Fig. 5(b), we first consider the Haldane phase fixed at $\phi = \pi/2$ and vary the on-site potential for $-\langle S^I_z\rangle$ and $\langle S^{II}_z\rangle$. The result for negative Haldane phase $\phi = -\pi/2$ is obtained by just making the replacement $-\langle S^I_z\rangle \leftrightarrow \langle S^{II}_z\rangle$. In the interval $-M_\alpha < G < M_\alpha$, the Chern number is $+2$. However, the bulk spin polarization changes sign and magnitude with the on-site potential. In the interval $M_\alpha < G < G_e$, the Chern number is -1. Interestingly, the bulk spin-polarization keeps its sign. That is, near $\phi = \pm\pi/2$, both the site-I and site-II bulk spin polarization indeed vary with the on-site potential, and keep their signs even when the Chern number has changed. To see the bulk-edge correspondence explicitly for spin-polarization, we will in the following focus only on the Haldane phases $\phi = \pi/2$ and $\phi = -\pi/2$, which have the largest phase regimes.

To confirm the above two distinct results deduced from the tight-binding Hamiltonian, we calculate the spin polarization of each edge current versus the on-site potential at the two different Haldane phases ($\phi = \pi/2$ and $\phi = -\pi/2$). The wave function is $\psi = (\psi_{I1\uparrow}, \psi_{I1\downarrow}, \psi_{II1\uparrow}, \psi_{II1\downarrow}, \psi_{I2\uparrow}, \psi_{I2\downarrow}, \cdots)^T$ and the spin polarization P_z is given by $P_z = |\psi_{I1\uparrow}|^2 - |\psi_{I1\downarrow}|^2 + |\psi_{II1\uparrow}|^2 - |\psi_{II1\downarrow}|^2 + \cdots$. The numerical results for the spin polarization of the edge currents for the positive ($\phi = +\pi/2$) and negative ($\phi = -\pi/2$) Haldane phases are shown in Fig. 6(a) and (b), respectively.

Consider the positive Haldane phase [see Fig. 6(a)]. As the on-site potential increases from $-M_\alpha$ to M_α, the spin polarization of the edge currents B and D increases. However, the spin polarization of the edge states A and C decreases. Interestingly, as the on-site potential passes through M_α and $-M_\alpha$, the direction of the spin polarization does not change at each edge of the ribbon, even though the chirality of the Chern number has changed from $+2$ to -1. This phenomenon is the same for the negative Haldane phase shown in Fig. 5(b).

Importantly, compare Figs. 5(b) and 6(a) at $\phi = \pi/2$. We find that the edge states B, D, A' behave like $\langle S^{II}_z\rangle$ and that the edge states A, C, B' behave like $-\langle S^I_z\rangle$ for a positive Haldane phase. The contributions of site-I and site-II to the spin polarization of the edge currents at $\phi = \pi/2$ are shown in Fig. 6(c) and (d). Here, the spin polarization is calculated only for one site, i.e., $P_z = |\psi_{I1\uparrow}|^2 - |\psi_{I1\downarrow}|^2 + |\psi_{I2\uparrow}|^2 - |\psi_{I2\downarrow}|^2 + \cdots$ for site-I and $P_z = |\psi_{II1\uparrow}|^2 - |\psi_{II1\downarrow}|^2 + |\psi_{II2\uparrow}|^2 - |\psi_{II2\downarrow}|^2 + \cdots$ for site-II. Figure 6(c) shows that the spin polarization of edge states A, C, and B' at site-I is larger than at site-II. Figure 6(d) shows that at a positive Haldane phase, the

[2] This can be seen as follows. By eliminating $(Z_+ + Z_-)/2$ [see Eq. (4)] in the Hamiltonian Eq. (2), the diagonal term becomes $\pm[G - (Z_- - Z_+)/2]$ and $Z_- - Z_+$ is proportional to $\sin\phi$, which is an odd function in ϕ. Therefore, the Haldane phase behaves like an effective magnetic field.

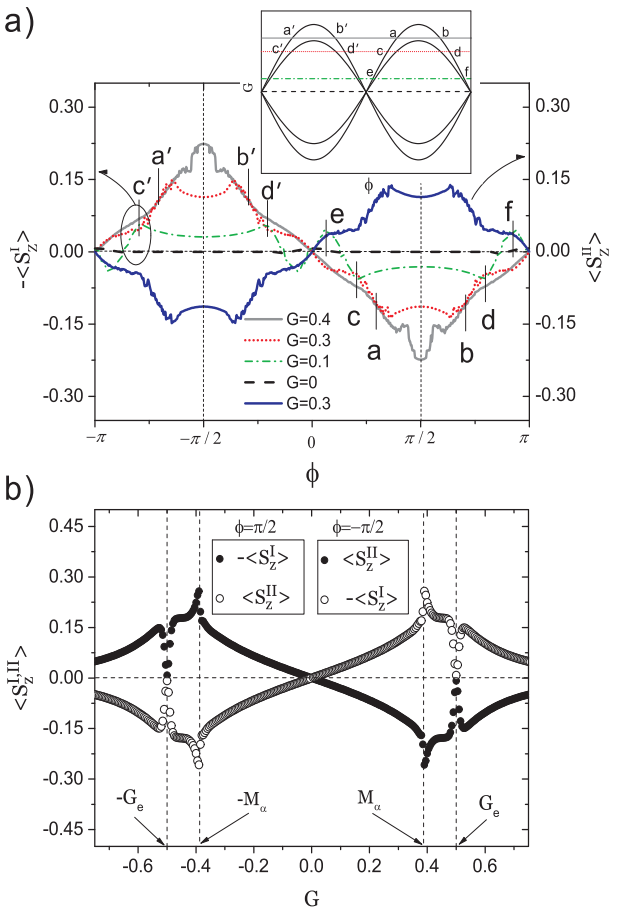

FIG. 5: (Color online) Linear response of $-S_z^I$ and S_z^{II} to an applied electric field. $\alpha = 0.7$ and $t_2 = 1/(6\sqrt{3})$. (a) Various Haldane phases and a discrete on-site potential and (b) various on-site potentials and a positive Haldane phase $\phi = \pi/2$ ($-\langle S_z^I\rangle \to \bullet$, $\langle S_z^{II}\rangle \to \circ$) and a negative Haldane phase $\phi = -\pi/2$ ($-\langle S_z^I\rangle \to \circ$, $\langle S_z^{II}\rangle \to \bullet$).

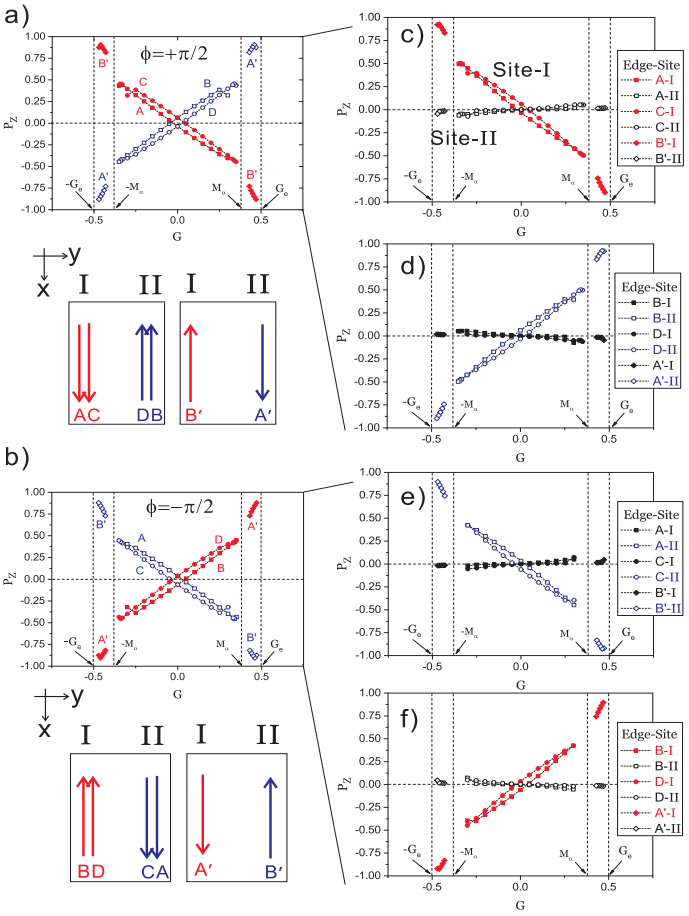

FIG. 6: (color online) Numerical results ($\alpha = 0.7$ and $t_2 = 1/(6\sqrt{3})$) for the change in spin polarization of the edge states for (a) $\phi = \pi/2$ and (b) $\phi = -\pi/2$ at $E_F = 0.01$. Filled and red (empty and blue) circle or square represent the edge states at left (right) hand side of ribbon. Panels (c) and (d) show the contributions of different sites (site-I and site-II) to the spin polarization of the edge states in (a). Panels (c) and (d) show that the large component for A, C, B' is site-I. However, the large component for B, D, A' is site-II.

spin polarization of B, D, and A' at site-II is indeed larger than that at site-I. We find that the spin polarization at site-II (site-I) is the large component and at site-I (site-II) is the small component for the edge states B, D, A' (A, C, B') for a positive Haldane phase. On the other hand, we also find that for a negative Haldane phase [see Figs. 6(b) and 5(b)] the spin polarization of site-II is the large component for A, C, B' [see Fig. 6(e)], and the spin polarization of site-I is the large component for the edge states B, D, A' [see Fig. 6(e)].

The spin polarization of the edge current at the right hand side of the ribbon [compare to Fig. 1] has a large contribution from site-II, and the opposite side of the ribbon has a large contribution from site-I. Furthermore, the sign of the spin polarization of the edge current is the same as the bulk spin polarization and is determined by the on-site potential, which is the approximate bulk-edge correspondence of spin polarization. We find that the spin polarization of the edge currents indeed persists regardless of the change in the Chern number, because the on-site potential behaves like an effective magnetic field and the Haldane current loops contribute unequally to the edges of the ribbon.

The spin polarization [Fig. 6] and current distribution [Fig. 4] for varying Haldane phase and on-site potential in real space is schematically summarized in Fig. 7(a) and (b).

If the on-site potential is fixed, a change in the Haldane phase leads to a change in the sign of the spin polarization and the direction of the edge current. However, if the Haldane phase is fixed, a change in the sign of the on-site potential leads only to a change in the sign of the spin polarization. Once the sign of the on-site potential is fixed, the spin polarization persists under a change in the Chern number. In this sense, the bulk-protected spin

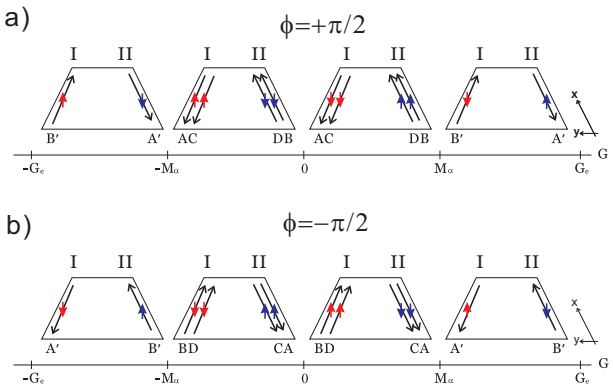

FIG. 7: (Color online) Schematic diagram showing the edge state current distribution (long arrows) and spin polarization for (a) a positive Haldane phase $\phi = \pi/2$ and (b) a negative Haldane phase $\phi = -\pi/2$.

polarization of the edge states in the Haldane-Rashba system can be controlled in a Chern-insulating phase. Furthermore, by varying the sign of the Haldane phase and the magnitude of the on-site potential, the current can be reduced without changing the polarization of spin.

The present result is rather different from the Kane-Mele-Rashba system [16] where the spin polarization in quantum spin-Hall phase persists in the presence of an exchange field in zero Chern number regime. Here, we study the spin polarization in non-zero Chern number regimes. The Haldane orbital Hamiltonian in Ref. [16] describes the coupling of the orbital angular momentum and the exchange field in which ν_{ij} behaves like an effective orbital angular momentum and does not cause the Haldane phase ϕ. In this paper, the Haldane phase ϕ plays an important role in changing the spin polarization and non-zero Chern number regimes. We emphasize that in this paper the orientation of spin polarization of edge currents can be controlled in a single and non-zero Chern-insulating phase.

In short, the Haldane current loop naturally determines the contribution of site atoms in a zigzag ribbon to the spin polarization of the edge currents. The on-site potential plays the role of an effective magnetic field, and the variation of the spin polarization of the edge state approximately obeys the bulk spin polarization of the site atoms near $\phi = \pm\pi/2$, which forms the approximate bulk-edge correspondence to the spin polarization. When ϕ approaches 0 and $\pm\pi$, the competition of the on-site potential and Haldane hopping term may break the correspondence. Because of the bulk protected spin polarization, the orientation of the spin polarization can be manipulated in a single and non-zero Chern-insulating phase.

V. CONCLUSION

We have investigated the Chern number pattern of the Haldane-Rashba system by using the Pontryagin winding number and numerical Berry curvature methods. We found that the on-site potential is the generator of the band-touching phenomenon and can be used to change the Chern number of the system. Three Chern insulating regimes can be exhibited by tuning the on-site potential. The Chern number pattern is $\{+2, -1, 0\}$ for positive Haldane phase and $\{-2, +1, 0\}$ for negative Haldane phase. If the on-site potential is fixed, the change in sign of the Haldane phase changes the direction of the edge currents and the sign of the out-of-plane spin polarization. Interestingly, we found that the spin polarization of the edge states persists under the change in the Chern number. Furthermore, the spin polarization of the edge states vary with the on-site potential, which implies that the on-site potential effectively couples to the spin of the edge states and behaves like an effective magnetic field. We calculated the bulk spin polarization and found that the spin polarization of the edge states approximately follows the bulk spin polarization. This indicates that the zigzag ribbon with two different Haldane current loops exhibits an approximate bulk-edge correspondence to the spin polarization. We found that the orientation of the spin polarization of the edge states could vary in a single Chern-insulating phase by tuning the on-site potential, which would play a crucial role in spintronics.

ACKNOWLEDGMENTS

T. W. C. would like to thank S. Murakami for valuable discussions regarding the Chern number and W.-X. Feng for the topological insulator. T. W. C and C. D. H thank the Taiwan Ministry of Science and Technology for financial support under Grant No. MOST 104-2112-M-110-003 and NSC 101-2112-M-002-016-MY3.

[1] M. Berry, Proc. Royal Soc. London, Ser. A **392**, 45 (1984).
[2] D. J. Thouless, M. Kohmoto, M. P. Nightingale, and M. den Nijs, Phys. Rev. Lett. **49**, 405 (1982). S. S. Chern, Ann. Math. **47**, 85 (1946).
[3] Y. Hatsugai, Phys. Rev. Lett. **71**, 3697 (1993); Y. Hatsugai, Phys. Rev. B **48**, 11851 (1993); H. Watanabe, Y. Hatsugai, and H. Aoki, Phys. Rev. B **82**, 241403(R) (2010).
[4] F. D. M. Haldane, Phys. Rev. Lett. **61**, 2015 (1988).
[5] C. L. Kane and E. J. Mele, Phys. Rev. Lett. **95**, 2266801 (2005); C. Xu and J. E. Moore, Phys. Rev. B **73**, 045322 (2006).
[6] B. A. Bernevig, T. L. Hughes, and S.-C. Zhang, Science **314**, 1757 (2006); M. Konig *et al.*, Science **318**, 766 (2007).

[7] L. Fu, C. L. Kane, and E. J. Mele, Phys. Rev. Lett. **98**, 106803 (2007); J. E. Moore and Balents, Phys. Rev. B **75**, 121306 (2007); R. Roy, Phys. Rev. B **79**, 195322 (2009); L. Fu and C. L. Kane, Phys. Rev. B **76**, 045302 (2007).

[8] D. Hsieh, D. Qian, L. Wray, Y. Xia, Y. S. Hor, R. J. Cava, and M. Z. Hasan, Nature (London) **452**, 970 (2008).

[9] M. Z. Hasan and C. L. Kane, Rev. Mod. Phys. **82**, 3045 (2010); X.-L. Qi and S.-C. Zhang, Rev. Mod. Phys. **83**, 1057 (2011).

[10] D. N. Sheng, Z. Y. Weng, L. Sheng, and F. D. M. Haldane, Phys. Rev. Lett. **97**, 036808 (2006).

[11] E. Prodan, Phys. Rev. B **80**, 125327 (2009); E. Prodan, New J. Phys. **12**, 065003 (2010). H. Li, L. Sheng, D. N. Sheng, and D. Y. Xing, Phys. Rev. B **82**, 165104 (2010).

[12] W.-Y. Shan, H.-Z. Lu, and S.-Q. Shen, New J. Phys. **12**, 043048 (2010); T. Fukui and Y. Hatsugai, Phys. Rev. B **75**, 121403 (2007); A. M. Essin and J. E. Moore, Phys. Rev. B **76**, 165307 (2007).

[13] B. Zhou, H.-Z. Lu, R.-L. Chu, S.-Q. Shan, and Q. Niu, Phys. Rev. Lett. **101**, 246807 (2008).

[14] Z. Qiao, S. A. Yang, W. Feng, W.-K. Tse, J. Ding, Y. Yao, J. Wang, and Q. Niu, Phys. Rev. B **82**, 161414(R) (2010).

[15] Y. Yang, Z. Xu, L. Sheng, B. Wang, D. Y. Xing, and D. N. Sheng, Phys. Rev. Lett. **107**, 066602 (2011).

[16] T.-W. Chen, Z.-R. Xiao, D.-W. Chiou and G.-Y. Guo, Phys. Rev. B **84**, 165453 (2011).

[17] E. Y. Ma, M. R. Calvo, J. Wang, B. Lian, M. Muhlbauer, C. Brune, Y.-T. Cui, K. Lai, W. Kundhikanjana, Y. Yang, M. Baenninger, M. König, C. Ames, H. Buhmann, P. Leubner, L. W. Molenkamp, S.-C. Zhang, D. Goldhaber-Gordon, M. A. Kelly, and Z.-X. Shen, Nature Comm. **6**, 7252 (2015).

[18] L. B. Shao, S.-L. Zhu, L. Sheng, D. X. Xing, and Z. D. Wang, Phys. Rev. Lett. **101**, 246801 (2008).

[19] X.-J. Liu, K. T. Law, T. K. Ng, and Patrick A. Lee, Phys. Rev. Lett. **111**, 120402 (2013).

[20] G. Jotzu, M. Messer, R. Desbuquois, M. Lebrat, T. Uehlinger, D. Greif, and T. Esslinger, Nature, **515**, 237 (2014).

[21] M. Zarea and N. Sandle, Phys. Rev. B **79**, 165442 (2009).

[22] W.-Y. Hsiang and D.-H. Lee, Phys. Rev. A **64**, 052101 (2001).

[23] D. Sticlet, F. Piechon, J.-N. Fuchs, P. Kalugin, and P. Simon, Phys. Rev. B **85**, 165456 (2012).

[24] S. Murakami, Prog. Theor. Phys. Suppl. **176**, 279 (2008); M. Oshikawa, Phys. Rev. B **50**, 17357 (1994);Y. Hatsugai, M. Kohmoto, and Y.-S. Wu, Phys. Rev. B **54**, 4898 (1996).

[25] Bo Yang, Phys. Rev. B **91**, 241403(R) (2015).